석사학위논문

Master's Thesis

Hellinger-Reissner 범함수를 이용한 판 유한요소의 개발

Development of the plate elements based on the Hellinger-Reissner functional

KOREA ADVANCED INSTITUTE OF SCIENCE AND TECHNOLOGY
KAIST
한국과학기술원
SINCE 1971

이 윤 규(李 淪 圭 Lee, Youn Gyu)

기계항공시스템학부 해양시스템공학전공

Division of Ocean Systems Engineering

School of Mechanical, Aerospace and Systems Engineering

KAIST

2011

Hellinger-Reissner 범함수를 이용한 판 유한요소의 개발

Development of the plate elements based on the Hellinger-Reissner functional

KAIST

Development of the plate elements based on the Hellinger-Reissner functional

Advisor : Professor Phill-Seung Lee

Co-advisor : Professor K. C. Park

by

Youn Gyu Lee

Division of Ocean Systems Engineering
School of Mechanical, Aerospace and Systems Engineering
KAIST

A thesis submitted to the faculty of KAIST in partial fulfillment of the requirements for the degree of Master of Science in Engineering in the School of Mechanical, Aerospace and Systems Engineering, Division of Ocean Systems Engineering. The study was conducted in accordance with Code of Research Ethics[1]

December 10, 2010

Approved by

Professor Phill-Seung Lee

_____

[1]Declaration of Ethical Conduct in Research**:** I, as a graduate student of KAIST, hereby declare that I have not committed any acts that may damage the credibility of my research. These include, but are not limited to: falsification, thesis written by someone else, distortion of research findings or plagiarism. I affirm that my thesis contains honest conclusions based on my own careful research under the guidance of my thesis advisor.

Development of the plate elements based on the Hellinger-Reissner functional

Youn Gyu Lee

The present dissertation has been approved by the dissertation committee as a master's thesis at KAIST

December 10, 2010

KAIST

Committee head Phill-Seung Lee

Committee member K. C. Park

Committee member Hyun Chung

MOSE
20093390

이 윤 규. Lee, Youn Gyu. Development of the plate elements based on the Hellinger-Reissner functional. Hellinger-Reissner 범함수를 이용한 판 유한요소의 개발. School of Mechanical, Aerospace and Systems Engineering, Division of Ocean Systems Engineering. 2011. 36p. Advisor Prof. Lee, Phill-Seung, Prof. Co-Advisor Park, Kwang-Chun. Text in English

ABSTRACT

The finite element method has been an effective tool to analyze plate structures. Low-order plate elements still have accuracy problems compared to high-order plate elements, particularly triangular plate elements. The objective of this study is to design a 3-node plate element based on the Hellinger-Reissner functional to obtain better performance. Numerical tests and convergence curves of the present 3-node element has been carried out, which illustrate a favorable convergence rate of the present 3-node plate element.

Keywords: Plate elements; Hellinger-Reissner functional; Finite element; Shear locking

KAIST

Table of Contents

KAIST

List of Tables

KAIST

List of Figures

KAIST

Chapter 1. Introduction

A plate is a structural element with plane dimensions larger than its thickness and is subjected to loads that cause bending deformation. Accordingly, the plate is widely used for a variety of engineering applications. The finite element method has been a powerful tool to analyze plate structures. Many researchers have developed the plate elements. However, it is still difficult to develop effective plate elements to increase the accuracy of the analysis of plates [1, 2].

As the plate thickness becomes smaller, the plate element is more sensitive depending on the plate geometry, loading and boundary conditions. This is the shear locking. The spurious shear stresses are predicted. These spurious shear stresses result in a strong artificial stiffening of the elements. Particularly, displacement-based plate elements produce shear locking extremely for bending-dominated plate structures in the case that the thickness is small. The convergence depends on the ratio of the plate thickness to characteristic length decreases [1-4].

The mixed-interpolated tensorial components(MITC) has been used to make the plate elements effective to the shear locking problems. The way of the MITC is that the proper strain interpolations are selected with a given displacement interpolation and then the particular typing points are chosen to express the strains based on the displacements. The quadratic MITC plate element is uniformly optimal, have a mathematical foundation for linear plate analysis. The MITC4 plate element based on the bilinear displacement interpolations is also uniformly optimal, but has somewhat less performance compared to the MITC9 plate element [5-10]. The MITC3 plate element degenerated from the MITC3 shell element is not uniformly optimal due to the shear locking. It is still the challenge to make the 3-node triangular plate elements uniformly optimal specially [11-13]. That's why we focus on the 4-node and 3-node plate element in this paper.

The important conditions exist to obtain an ideal plate element. The formulation should satisfy the following conditions. One of the conditions is that the ellipticity which explains that the finite element discretization under the unsupportable boundary condition physically represent the exact rigid body modes without the spurious zero energy mode. The plate element should have three zero energy modes. Under the free-free boundary condition, the plate elements have three rigid body modes because the zero energy mode corresponds to the rigid body mode. This condition can be identified from how many zero eigenvalues of the stiffness matrix of the single unsuppoerted plate element there are. Another condition is the consistency. The solution of the finite element discretizations should convergence to the mathematical solution as the size of the element gets to zero. When h approaches zero, the bilinear forms of the finite element discretixation should be the bilinear forms of the mathematical model because the bilinear forms of the finite element discretization can be a function of the element size h. The other thing is that Inf-sup condition strongly relative to a mixed finite element discretization. To satisfy Inf-sup condition, the plate element should be independent of the plate thickness to have the accuracy solution without shear locking. Inf-sup condition represents that the convergence should be uniformly optimal in bending-dominated plate problems [12, 15].

KAIST

It is necessary to set up the practical requirements to develop the plate element because it is so difficult to satisfy all of the conditions perfectly. There are the practical requirements for the plate element. The first requirement is to have no spurious zero energy mode in connected with the ellipticity condition. The second thing is to be free shear locking in plate bending problems. The third is that convergence curve should be uniformly optimal in the reasonable range of the ratio the thickness to the characteristic length. The fourth is to be a spatial isotropy independent of the sequence of node numbering [12].

The purpose of this study is to develop 4-node and 3-node plate elements with the Hellinger-Reissner functional to satisfy the practical requirements. The method to develop the finite elements using the Hellinger-Reissner functional is so successful because this functional can make the displacements and the strains independent. The poor strain fields from the displacement-based formulation can be changed to the richer strain fields from interpolating the strains independently. Then we can use static condensation on the strain to get the stiffness matrix [1].

This research could be useful to increase the computational efficiency and make the triangular mesh patterns of the model getting more universal. The 4-node and 3-node plate elements use the smallest number of the nodes among the plate elements. This is the advantage of the low order elements at the view of the computational cost if the element is uniformly optimal. The triangular mesh is so good when modeling the curved or complex structure. But the quadrilateral mesh has been still used due to the better performance. If the ideal triangular elements are developed, the triangular mesh will be getting more general for the finite element discretizations.

In the following the sections, at first we report that how the plate formulation is derived from the Hellinger-Reissner functional with several kinds of the transverse shear strain interpolations, then the numerical results are shown to verify the performance of the plate elements. Finally, We have discussions about the results in the conclusion.

KAIST

Chapter 2. Formulation

The plate element formulation is based on the Reissner/Mindlin theory that shear deformations are included. The line originally normal to the midsurface in general does not remain perpendicular to the midsurface during the deformations [14].

2.1. Displacement-based formulation

The variational indicator corresponding to the Reissner/Mindlin plate is, in linear elastic static analysis,

KAIST

$$\Pi = \frac{1}{2}\int_A \boldsymbol{\kappa}^T \mathbf{C_b} \boldsymbol{\kappa} dA + \frac{1}{2}\int_A \boldsymbol{\gamma}^T \mathbf{C_s} \boldsymbol{\gamma} dA - \int_A w p dA \tag{1}$$

where

$$\boldsymbol{\kappa} = \begin{bmatrix} \frac{\partial \beta_x}{\partial x} \\ \frac{\partial \beta_y}{\partial y} \\ \frac{\partial \beta_x}{\partial y} + \frac{\partial \beta_y}{\partial x} \end{bmatrix} \tag{2}$$

$$\boldsymbol{\gamma} = \begin{bmatrix} \frac{\partial w}{\partial x} - \beta_x \\ \frac{\partial w}{\partial y} - \beta_y \end{bmatrix} \tag{3}$$

$$\mathbf{C_b} = \frac{Et^3}{12(1-\nu^2)} \begin{bmatrix} 1 & \nu & 0 \\ \nu & 1 & 0 \\ 0 & 0 & \frac{1-\nu}{2} \end{bmatrix}; \qquad \mathbf{C_s} = \frac{Etk}{2(1+\nu)} \begin{bmatrix} 1 & 0 \\ 0 & 1 \end{bmatrix} \tag{4}$$

and, w is the transverse displacement and β_x and β_y are the rotations of the normal to the undeformed middle surface in the x, z and y, z planes, respectively, p is the transverse loading per unit of the midsurface area A, t is the thickness of the plate(assumed constant). Also, E is Young's modulus, ν is Poisson's ratio and k is a shear correction factor. The displacement of the element is obtained by

$$w = \sum_{i=1}^{q} h_i w_i; \quad \beta_x = -\sum_{i=1}^{q} h_i \theta_y^i; \quad \beta_y = \sum_{i=1}^{q} h_i \theta_x^i \tag{5}$$

where w_i, θ^i_y and θ^i_x are the nodal point values of the variables w, β_x and β_y, respectively, the h_i are the interpolation functions and q is the number of nodes of the elements. The shear locking occurs in the formulation because the transverse shear strains exist under a constant bending moment. In other words this finite element discretization does not include the Kirchhoff plate assumptions [14].

2.2. Mixed Formulation with the Hellinger-Reissner functional

KAIST

The Hellinger-Reissner functional is introduced to use static condensation

$$\Pi_{HR} = \int_V \left(-\frac{1}{2} \boldsymbol{\epsilon}^T \mathbf{C} \boldsymbol{\epsilon} + \boldsymbol{\epsilon}^T \mathbf{C} \boldsymbol{\partial}_{\boldsymbol{\epsilon}} \mathbf{u} - \mathbf{u}^T \mathbf{f}^{\mathbf{B}} \right) dV + \text{boundary terms} \tag{6}$$

$$\boldsymbol{\partial}_{\boldsymbol{\epsilon}} = \begin{bmatrix} \frac{\partial}{\partial x} & 0 & 0 \\ 0 & \frac{\partial}{\partial y} & 0 \\ 0 & 0 & \frac{\partial}{\partial z} \\ \frac{\partial}{\partial y} & \frac{\partial}{\partial x} & 0 \\ 0 & \frac{\partial}{\partial z} & \frac{\partial}{\partial y} \\ \frac{\partial}{\partial z} & 0 & \frac{\partial}{\partial x} \end{bmatrix} \tag{7}$$

where $\boldsymbol{\epsilon}$ is strains, $\mathbf{u}$ is displacements, $\mathbf{C}$ is the stress-strain matrix and $\mathbf{f^B}$ is the body force. $\boldsymbol{\partial}_{\boldsymbol{\epsilon}}$ represents the differential operator on $\mathbf{u}$, see Ref. [1]. In the plate formulation the Hellinger-Reissner functional is changed.

$$\overline{\Pi}_{\mathrm{HR}} = \int_{\mathrm{A}} \left(\frac{1}{2} \boldsymbol{\kappa}^{\mathrm{T}} \mathbf{C_b} \boldsymbol{\kappa} - \frac{1}{2} \boldsymbol{\gamma}^{\mathbf{A}^{\mathrm{T}}} \mathbf{C_s} \boldsymbol{\gamma}^{\mathbf{A}} + \boldsymbol{\gamma}^{\mathbf{A}^{\mathrm{T}}} \mathbf{C_s} \boldsymbol{\gamma} - \mathbf{u}^{\mathrm{T}} \mathbf{p} \right) \mathrm{dA} + \text{boundary terms} \tag{8}$$

where $\boldsymbol{\kappa}$ is the section curvatures, $\boldsymbol{\gamma}$ is the transverse shear strains and $\boldsymbol{\gamma}^{\mathbf{A}}$ is the approximated transverse shear strain field.

Invoking $\delta\overline{\Pi}_{\mathrm{HR}} = 0$

$$\int_{\mathrm{A}} (\delta \boldsymbol{\kappa}^{\mathrm{T}} \mathbf{C_b} \boldsymbol{\kappa} + \delta \boldsymbol{\gamma}^{\mathrm{T}} \mathbf{C_s} \boldsymbol{\gamma}^{\mathbf{A}}) \mathrm{dA} = \int_{\mathrm{A}} \delta \mathbf{u}^{\mathrm{T}} \mathbf{p} \mathrm{dA} \tag{9}$$

$$\int_{\mathrm{A}} \delta \boldsymbol{\gamma}^{\mathbf{A}^{\mathrm{T}}} \mathbf{C_s} (\boldsymbol{\gamma} - \boldsymbol{\gamma}^{\mathbf{A}}) \mathrm{dA} = 0 \tag{10}$$

Eq. (9) and Eq. (10) are changed to the matrix form

$$\begin{bmatrix} \mathbf{K_{uu}} & \mathbf{K_{u\epsilon}} \\ \mathbf{K_{u\epsilon}^{T}} & \mathbf{K_{\epsilon\epsilon}} \end{bmatrix} \begin{bmatrix} \mathbf{U} \\ \boldsymbol{\alpha} \end{bmatrix} = \begin{bmatrix} \mathbf{R_B} \\ \mathbf{0} \end{bmatrix} \tag{11}$$

KAIST

where

$$\mathbf{K_{uu}} = \int_{\mathrm{A}} \delta \boldsymbol{\kappa}^{\mathrm{T}} \mathbf{C_b} \boldsymbol{\kappa} \mathrm{dA} \tag{12}$$

$$\mathbf{K_{u\epsilon}} = \int_{\mathrm{A}} \delta \boldsymbol{\gamma}^{\mathrm{T}} \mathbf{C_s} \boldsymbol{\gamma}^{\mathbf{A}} \mathrm{dA} \tag{13}$$

$$\mathbf{K_{\epsilon\epsilon}} = -\int_{\mathrm{A}} \delta \boldsymbol{\gamma}^{\mathbf{A}^{\mathrm{T}}} \mathbf{C_s} \boldsymbol{\gamma}^{\mathbf{A}} \mathrm{dA} \tag{14}$$

Let

$$\mathbf{u} = \mathbf{HU}; \quad \boldsymbol{\kappa} = \mathbf{B_b U}; \quad \boldsymbol{\gamma} = \mathbf{B_s U}; \quad \boldsymbol{\gamma}^{\mathbf{A}} = \mathbf{B_s^A} \boldsymbol{\alpha} \tag{15}$$

where $\mathbf{H}$ is the isoparametric displacement interpolation matrix, $\mathbf{U}$ is the nodal displacement vector, $\mathbf{B_b}$ is

the curvature-displacement matrix, $\mathbf{B_s}$ is the transverse shear strain-displacement matrix, $\mathbf{B_s^A}$ is the approximated transverse shear strain matrix and $\boldsymbol{\alpha}$ is the vector of the transverse strain parameters. The final stiffness matrix is obtained using static condensation on $\boldsymbol{\alpha}$

$$\mathbf{K} = \mathbf{K_{uu}} - \mathbf{K_{u\epsilon}}\mathbf{K_{\epsilon\epsilon}^{-1}}\mathbf{K_{u\epsilon}^{T}} \tag{16}$$

where

$$\mathbf{K_{uu}} = \int_A \mathbf{B_b^T C_b B_b} \mathrm{Det}(\mathbf{J}) \mathrm{dA} \tag{17}$$

$$\mathbf{K_{u\epsilon}} = \int_A \mathbf{B_s^T C_s B_s^A} \mathrm{Det}(\mathbf{J}) \mathrm{dA} \tag{18}$$

$$\mathbf{K_{\epsilon\epsilon}} = -\int_A \mathbf{B_s^{A^T} C_s B_s^A} \mathrm{Det}(\mathbf{J}) \mathrm{dA} \tag{19}$$

where **J** is the jacobian operator matrix. The matrix $\mathbf{B_b}$ is calculated by the displacement-based formulation

$$\boldsymbol{\kappa} = \begin{bmatrix} \frac{\partial \beta_x}{\partial x} \\ \frac{\partial \beta_y}{\partial y} \\ \frac{\partial \beta_x}{\partial y} + \frac{\partial \beta_y}{\partial x} \end{bmatrix} = \mathbf{B_b U} \, . \tag{20}$$

The plate elements from the Hellinger-Reissner functional are presented in Table 1.

2.2.1. The transverse shear strain-displacement matrix from the mixed formulation

The matrix $\mathbf{B_s}$ is calculated from the Mixed Interpolation of Tensorial Components. The $\tilde{\epsilon}_{rt}$ and $\tilde{\epsilon}_{st}$ are the strain tensors based on the covariant tensor components and contravariant base vectors for 4-node and 3-node plate elements. The strain tensor can be given by covariant tensor components and contravariant base vectors

$$\epsilon = \tilde{\epsilon}_{ij}\mathbf{g}^{\mathbf{i}}\mathbf{g}^{\mathbf{j}} \;\; ; \quad i,j \equiv r,s,t \tag{21}$$

where the tilde(~) means that the covariant tensor components come from the natural coordinate system. The covariant strain components are obtained by

$$\tilde{\epsilon}_{ij} = \frac{1}{2}(\mathbf{g}_{\mathbf{i}} \cdot \mathbf{u}_{,\mathbf{j}} + \mathbf{g}_{\mathbf{j}} \cdot \mathbf{u}_{,\mathbf{i}}) \tag{22}$$

where

$$\mathbf{g}_{\mathbf{r}} = \frac{\partial \mathbf{x}}{\partial r} \;\; ; \quad \mathbf{g}_{\mathbf{s}} = \frac{\partial \mathbf{x}}{\partial s} \;\; ; \quad \mathbf{g}_{\mathbf{t}} = \frac{t}{2}\mathbf{e}_{\mathbf{z}} \tag{23}$$

$$\mathbf{u}_{,\mathbf{i}} = \frac{\partial \mathbf{u}}{\partial r_i} \quad \text{with } r_1=r,\ r_2=s,\ r_3=t \tag{24}$$

We use

KAIST

$$\tilde{\epsilon}_{ij}\mathbf{g}^{\mathbf{i}}\mathbf{g}^{\mathbf{j}} = \epsilon_{k\ell}\mathbf{e}_{\mathbf{k}}\mathbf{e}_{\boldsymbol{\ell}} \tag{25}$$

Where the $\epsilon_{k\ell}$ are the components of the strain tensor in the Cartesian coordinate system [1]. We can calculate from Eq. (25)

$$\begin{bmatrix}\gamma_{xz}\\ \gamma_{yz}\end{bmatrix} = \begin{bmatrix}2\tilde{\epsilon}_{rt}(\mathbf{g}^{\mathbf{r}} \cdot \mathbf{e}_{\mathbf{x}})(\mathbf{g}^{\mathbf{t}} \cdot \mathbf{e}_{\mathbf{z}}) + 2\tilde{\epsilon}_{st}(\mathbf{g}^{\mathbf{s}} \cdot \mathbf{e}_{\mathbf{x}})(\mathbf{g}^{\mathbf{t}} \cdot \mathbf{e}_{\mathbf{z}})\\ 2\tilde{\epsilon}_{rt}(\mathbf{g}^{\mathbf{r}} \cdot \mathbf{e}_{\mathbf{y}})(\mathbf{g}^{\mathbf{t}} \cdot \mathbf{e}_{\mathbf{z}}) + 2\tilde{\epsilon}_{st}(\mathbf{g}^{\mathbf{s}} \cdot \mathbf{e}_{\mathbf{y}})(\mathbf{g}^{\mathbf{t}} \cdot \mathbf{e}_{\mathbf{z}})\end{bmatrix}. \tag{26}$$

• HR4M-LCS

We use the interpolations of the transverse shear strains to compose the matrix $\mathbf{B}_s$ for the HR4M-LCS plate element

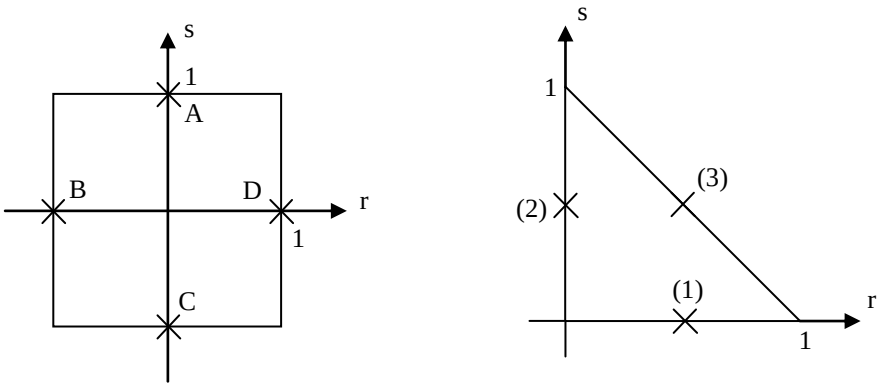

Fig. 1. Typing points for transverse shear strain interpolation. (a) for HR4M-LCS and MITC4 Plate element (b) for HR3M-LTCS and MITC3 Plate element.

$$\tilde{\epsilon}_{rt} = \frac{1}{2}(1+s)\tilde{\epsilon}_{rt}^{A} + \frac{1}{2}(1-s)\tilde{\epsilon}_{rt}^{C} \tag{27}$$

$$\tilde{\epsilon}_{st} = \frac{1}{2}(1+r)\tilde{\epsilon}_{st}^{D} + \frac{1}{2}(1-r)\tilde{\epsilon}_{st}^{B} \tag{28}$$

Where $\tilde{\epsilon}_{rt}^{A}, \tilde{\epsilon}_{rt}^{C}, \tilde{\epsilon}_{st}^{D}$ and $\tilde{\epsilon}_{st}^{B}$ are the transverse shear tensor components at points A, B, C and D calculated by Eq. (22)-(24). Fig. 1(a) shows the typing positions of the HR4M-LCS. Eq. (27) and (28) substitute into Eq. (26) to obtain the matrix $\mathbf{B_s}$ in the Cartesian coordinate system. The matrix $\tilde{\mathbf{B}}_{\mathbf{s}}^{\mathbf{A}}$ based on covariant tensor components and contravariant base vectors can be obtained from the approximated linear relationship [10]

$$\tilde{\boldsymbol{\epsilon}}^{\mathbf{A}} = \begin{bmatrix} \tilde{\epsilon}_{rt} \\ \tilde{\epsilon}_{st} \end{bmatrix} = \begin{bmatrix} \frac{1}{2}(1+s) & \frac{1}{2}(1-s) & 0 & 0 \\ 0 & 0 & \frac{1}{2}(1+r) & \frac{1}{2}(1-r) \end{bmatrix} \begin{bmatrix} \tilde{\alpha}_1 \\ \tilde{\alpha}_2 \\ \tilde{\alpha}_3 \\ \tilde{\alpha}_4 \end{bmatrix} = \tilde{\mathbf{B}}_{\mathbf{s}}^{\mathbf{A}} \tilde{\boldsymbol{\alpha}} \tag{29}$$

Eq. (29) should be substituted into Eq. (26) to obtain the $\mathbf{B_s}^{\mathbf{A}}$ based on the Cartesian coordinate system.

• HR3M-LTCS

We use the interpolations of the transverse shear strains to compose the matrix $\mathbf{B_s}$ for the HR3M-LTCS plate element

$$\tilde{\epsilon}_{rt} = \tilde{\epsilon}_{rt}^{(1)} + cs \tag{30}$$

$$\tilde{\epsilon}_{st} = \tilde{\epsilon}_{st}^{(2)} - cr \tag{31}$$

where

$$c = \tilde{\epsilon}_{st}^{(2)} - \tilde{\epsilon}_{rt}^{(1)} - \tilde{\epsilon}_{st}^{(3)} + \tilde{\epsilon}_{rt}^{(3)} \tag{32}$$

Where $\tilde{\epsilon}_{rt}^{(1)}, \tilde{\epsilon}_{st}^{(2)}, \tilde{\epsilon}_{rt}^{(3)}$ and $\tilde{\epsilon}_{s}^{(3)}$ are the transverse shear tensor components at points (1), (2) and (3) calculated by Eq. (22)-(24). The typing points are chosen at the center of the edges. Fig. 1(b) shows the typing positions of the HR3M-LTCS. Eq. (30) and (31) substitute into Eq. (26) to obtain the matrix $\mathbf{B_s}$ in the Cartesian coordinate system. The matrix $\tilde{\mathbf{B}}_{\mathbf{s}}^{\mathbf{A}}$ can consist of the approximated linear relationship with the isotropic condition [12]

$$\tilde{\boldsymbol{\epsilon}}^{\mathbf{AS}} = \begin{bmatrix} \tilde{\epsilon}_{rt} \\ \tilde{\epsilon}_{st} \end{bmatrix} = \begin{bmatrix} 1 & 0 & s \\ 0 & 1 & -r \end{bmatrix} \begin{bmatrix} \tilde{\alpha}_1 \\ \tilde{\alpha}_2 \\ \tilde{\alpha}_3 \end{bmatrix} = \tilde{\mathbf{B}}_{\mathbf{s}}^{\mathbf{A}} \tilde{\boldsymbol{\alpha}} \tag{33}$$

Eq. (33) should be substituted into Eq. (26) to obtain the $\mathbf{B_s}^{\mathbf{A}}$ based on the Cartesian coordinate system.

• HR4M-LCSR and HR3M-LTCSR

The matrix $\mathbf{B_s}$ of the HR4M-LCSR and HR3M-LTCSR is the same as that of the HR4M-LCS and HR3M-LTCS respectively. The matrix $\tilde{\mathbf{B}}_{\mathbf{s}}^{\mathbf{A}}$ can be established on the rotated contravariant base vectors

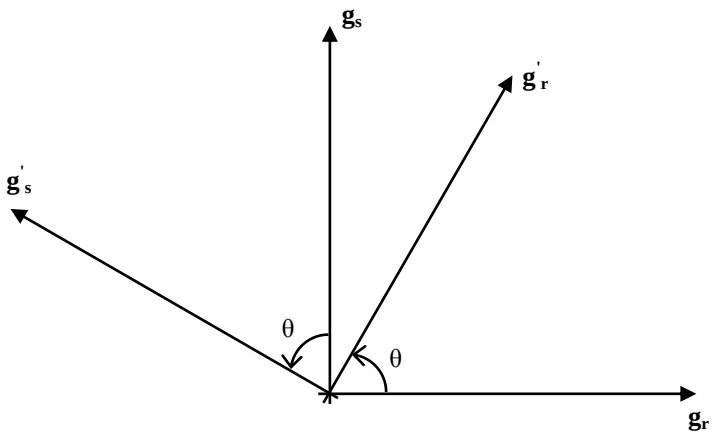

Fig. 2. Rotated covariant base vectors($\mathbf{g}'_r$ and $\mathbf{g}'_s$) and original covariant base vectors($\mathbf{g}_r$ and $\mathbf{g}_s$).

$$\begin{bmatrix} x' \\ y' \end{bmatrix} = \begin{bmatrix} \cos\theta & -\sin\theta \\ \sin\theta & \cos\theta \end{bmatrix} \begin{bmatrix} x \\ y \end{bmatrix} \tag{34}$$

KAIST

Where x and y are an original coordinate, θ is a counterclockwise angle about the origin of the Cartesian coordinate system. x' and y' are the rotated coordinate. The covariant base vectors are defined from the nodes rotated with Eq. (34) shown Fig. 2. The rotated contravariant base vectors $\mathbf{g}^{r'}$ and $\mathbf{g}^{s'}$ are calculated with the reciprocal metric tensor and the covariant base vectors.

To design the HR4M-LCSR Plate element, Eq. (29) based on $\mathbf{g}^{r'}$ and $\mathbf{g}^{s'}$ should be substituted into Eq. (26) to obtain the $\mathbf{B}_s^{\mathbf{A}}$ based on the Cartesian coordinate system. For the HR3M-LTCSR Plate element, Eq. (33) based on $\mathbf{g}^{r'}$ and $\mathbf{g}^{s'}$ should also be substituted into Eq. (26) to obtain the $\mathbf{B}_s^{\mathbf{A}}$ based on the Cartesian coordinate system.

2.2.2. The transverse shear strain-displacement matirx from the displacement-based formulation

The matrix $\mathbf{B}_s$ is obtained by the displacement-based formulation

$$\boldsymbol{\gamma} = \begin{bmatrix} \frac{\partial w}{\partial x} - \beta_x \\ \frac{\partial w}{\partial y} - \beta_y \end{bmatrix} = \mathbf{B_s U} \,. \tag{35}$$

• HR4-CCS, HR4-LCS, HR3-CCS and HR3-LTCS

The matrix $\widetilde{\mathbf{B}}_{\mathbf{s}}^{\mathbf{A}}$ can be obtained from the approximated constant relationship

$$\tilde{\boldsymbol{\epsilon}}^{\mathbf{A}} = \begin{bmatrix} \tilde{\epsilon}_{rt} \\ \tilde{\epsilon}_{st} \end{bmatrix} = \begin{bmatrix} 1 & 0 \\ 0 & 1 \end{bmatrix} \begin{bmatrix} \tilde{\alpha}_1 \\ \tilde{\alpha}_2 \end{bmatrix} = \widetilde{\mathbf{B}}_{\mathbf{s}}^{\mathbf{A}} \tilde{\boldsymbol{\alpha}} \tag{36}$$

For the HR4-CCS Plate element and HR3-CCS Plate element. Eq. (36) should be substituted into Eq. (26) to obtain the $\mathbf{B_s}^{\mathbf{A}}$ based on the Cartesian coordinate system. The matrix $\widetilde{\mathbf{B}}_{\mathbf{s}}^{\mathbf{A}}$ can be Eq. (29) and Eq. (33) for the HR4-LCS and HR3-LTCS respectively. The equations should also be substituted into Eq. (26).

KAIST

2.3. MITC Plate elements

The plate element based on the pure displacement discretization occurs the shear locking more strongly for a low-order element as the ratio of thickness and length decreases. In the MITC formulation, the bending and shear part of the stiffness matrix are obtained by the different interpolation to escape the shear locking. The bending strain-displacement matrix follows the formulation based on the pure displacement discretization. The transverse shear interpolations are obtained by the same way to calculate the $\mathbf{B_s}$ of the HR4M-LCS and the HR3M-LTCS for the MITC4 and MITC3 plate element respectively [12, 14].

Table 1. The plate elements based on the Hellinger-Reissner functional.

	Plate element	$\mathbf{B}_s$	$\mathbf{B}_s^A$
4 node	HR4-CCS	Displacement-based components [Eq. (35)]	Constant transverse Covariant Shear strain field [Eq. (36)]
	HR4-LCS		Linear transverse Covariant Shear strain field [Eq. (29)]
	HR4M-LCS	Mixed Interpolation of Tensorial Components [Eq. (27) and (28) → Eq. (26)]	Linear transverse Covariant Shear strain field [Eq. (29)]
	HR4M-LCSR		Linear transverse Covariant Shear strain field with Rotation [Eq. (29) and (34)]
3 node	HR3-CCS	Displacement-based components [Eq. (35)]	Constant transverse Covariant Shear strain field [Eq. (36)]
	HR3-LTCS		Linear transverse Triangular Covariant Shear strain field [Eq. (33)]
	HR3M-LTCS	Mixed Interpolation of Tensorial Components [Eq. (30) and (31) → Eq. (26)]	Linear transverse Triangular Covariant Shear strain field [Eq. (33)]
	HR3M-LTCSR		Linear transverse Triangular Covariant Shear strain field with Rotation [Eq. (33) and (34)]

KAIST

Chapter 3. Numerical results

A variety of numerical tests of the plate elements are presented in this section. The tested elements include HR4-CCS, HR4-LCS, HR4M-LCS, HR4M-LCSR, HR3-CCS, HR3-LTCS, HR3M-LTCS and HR3M-LTCSR. We verify the elements whether the requirements are satisfied. To check the performance of the elements, we suggest the simple convergence study with plate bending problems.

3.1. The requirements for plate elements

• Zero energy mode test. This test is based on checking out how many zero eigenvalues of the stiffness matrix there are. The zero eigenvalues correspond to the rigid body modes. The other eigenvalues match the staining modes. The plate element has three rigid body modes at the z-translation, x-rotation and y-rotation under one unsupported boundary conditions [12, 13]. The results of the zero energy mode test are presented in Table 5.

The general characteristic of the eigenvalues of the elements is that there is no spurious mode with the approximated linear transverse shear strain field and the element has spurious mode with the approximated constant transverse shear strain field. Particularly, the specific mode's eigenvalues of the HR4M-LCSR and the HR3M-LTCSR are changed by the variation of the angle defined in the approximated transverse shear strain field in Table 2 and 3. The eigenvalues of the ninth and tenth modes of the HR4M-LCSR decrease depending on increasing the angle. The eigenvalues of the seventh mode of the HR3M-LTCSR also decrease with increasing the angle. These order's modes are closely relative to the twisting strain energy mode. When the angle is 90 degrees specially, the spurious energy mode occurs in the HR4-LCSR and the HR3M-LTCSR. Note that the smaller eigenvalues the stiffness has, the more effective the element [1]. The HR4M-LCSR uses the angle 45 degrees even though the more angles make the element

more effective until 90 degrees. The reason is that the transverse shear stresses increase with the constant twisting stress as the angles increase in the twisting patch test. In the case of the HR3M-LCSR the angle 89 degrees is used to obtain more effective element with escaping the spurious mode.

We apply the pure twisting mode to only one element which includes HR4M-LCSR45, MITC4 plate element, HR3M-LTCSR89 and MITC3 plate element to verify the flexibility of the elements. The less strain energy is evaluated, the more flexible the element under the twisting mode. The twisting strain energy of the HR4M-LCSR45 and HR3M-LTCSR89 is smaller than that of MITC4 and MITC3 plate element respectively. The results of the twisting mode test are presented in Table. 4.

Table 2. The eigenvalues of the HR4M-LCSR with the variation of the angle(θ) defined in the matrix $\mathbf{B}_s^A$ (t/L=0.001, L=1.0, E=1.7472×10^7 and ν=0.3). The results come from one quadrilateral uniform mesh shown Fig. 4 (a).

Angle(θ) / mode	15°	30°	45°	60°	75°	90°	MITC4 plate
1	4.645E-13	-1.899E-12	-3.054E-12	-1.652E-12	-6.783E-12	-8.504E-14	-6.253E-13
2	1.656E-12	-8.828E-13	-1.902E-13	-1.052E-12	3.612E-13	-8.504E-14	2.996E-13
3	2.306E-12	-2.068E-14	1.584E-13	5.145E-12	3.612E-13	0.000E+00	8.330E-13
4	7.200E-04	7.200E-04	7.200E-04	7.200E-04	7.200E-04	2.896E-13	7.200E-04
5	7.200E-04	7.200E-04	7.200E-04	7.200E-04	7.200E-04	9.565E-13	7.200E-04
6	9.956E-04	9.956E-04	9.956E-04	9.956E-04	9.956E-04	7.200E-04	9.956E-04
7	1.120E-03	1.120E-03	1.120E-03	1.120E-03	1.120E-03	7.200E-04	1.120E-03
8	2.080E-03	2.080E-03	2.080E-03	2.080E-03	2.080E-03	1.120E-03	2.080E-03
9	5.225E+02	4.200E+02	2.800E+02	1.400E+02	3.751E+01	1.120E-03	5.600E+02
10	4.702E+03	3.780E+03	2.520E+03	1.260E+03	3.376E+02	2.080E-03	5.040E+03
11	8.400E+03	8.400E+03	8.400E+03	8.400E+03	8.400E+03	8.400E+03	8.400E+03
12	8.400E+03	8.400E+03	8.400E+03	8.400E+03	8.400E+03	8.400E+03	8.400E+03

Table 3. The eigenvalues of the HR3M-LTCSR with the variation of the angle(θ) defined in the matrix $\mathbf{B}_s^A$ (t/L=0.001, L=1.0, E=1.7472×10^7 and ν=0.3). The results come from one triangular regular mesh shown Fig. 4 (b)

Angle(θ) / mode	15°	30°	45°	60°	75°	89°	90°	MITC3 Plate
1	-2.413E-12	-2.428E-12	-2.255E-12	-2.039E-12	-6.227E-12	-2.862E-12	-3.060E-12	-2.456E-12
2	-9.633E-13	-8.929E-13	-1.353E-12	-1.008E-12	-2.514E-12	-1.022E-12	-1.380E-12	-8.121E-13
3	-4.332E-13	-3.717E-13	-3.340E-13	1.043E-12	-9.046E-13	-5.324E-13	-3.205E-13	-6.588E-13
4	6.676E-04	6.676E-04	6.676E-04	6.676E-04	6.676E-04	6.676E-04	6.899E-13	6.676E-04
5	8.145E-04	8.145E-04	8.145E-04	8.145E-04	8.145E-04	8.127E-04	6.676E-04	8.145E-04
6	2.492E-03	2.492E-03	2.492E-03	2.492E-03	2.492E-03	2.492E-03	1.075E-03	2.492E-03
7	3.446E+02	2.770E+02	1.847E+02	9.238E+01	2.476E+01	1.128E-01	2.492E-03	3.693E+02
8	4.670E+03	4.670E+03	4.669E+03	4.668E+03	4.667E+03	4.667E+03	4.667E+03	4.671E+03
9	1.176E+04	1.176E+04	1.176E+04	1.176E+04	1.176E+04	1.176E+04	1.176E+04	1.176E+04

Table 4. Constant twisting mode test of HR4M-LCSR45, MITC4 plate , HR3M-LTCSR89 and MITC3 plate (L=1.0, E=1.7472×10^7 and ν=0.3). The results come from one quadrilateral and triangular mesh in Fig. 4. The constant twisting mode of the 4-node and 3-node plate element is [0 0 0 0;-1 1 1 -1;-1 -1 1 1] and [0 0 0; 1 -1 0; 1 0 -1] respectively. The modes are normalized.

plate / t/L	4-node element		3-node element	
	HR4M-LCSR45	MITC4 plate	HR3M-LTCSR89	MITC3 plate
0.01	1.400E+03	2.800E+03	2.340E+02	2.100E+03
0.001	1.400E+02	2.800E+02	2.339E+01	2.100E+02
0.0001	1.400E+01	2.800E+01	2.339E+00	2.100E+01

* The nodal displacement vector of the 4-node and 3-node plate element is [w_1, w_2, w_3, w_4;θ_x^1, θ_x^2, θ_x^3, θ_x^4; θ_y^1, θ_y^2, θ_y^3, θ_y^4] and [w_1, w_2, w_3;θ_x^1, θ_x^2, θ_x^3; θ_y^1, θ_y^2, θ_y^3] respectively.

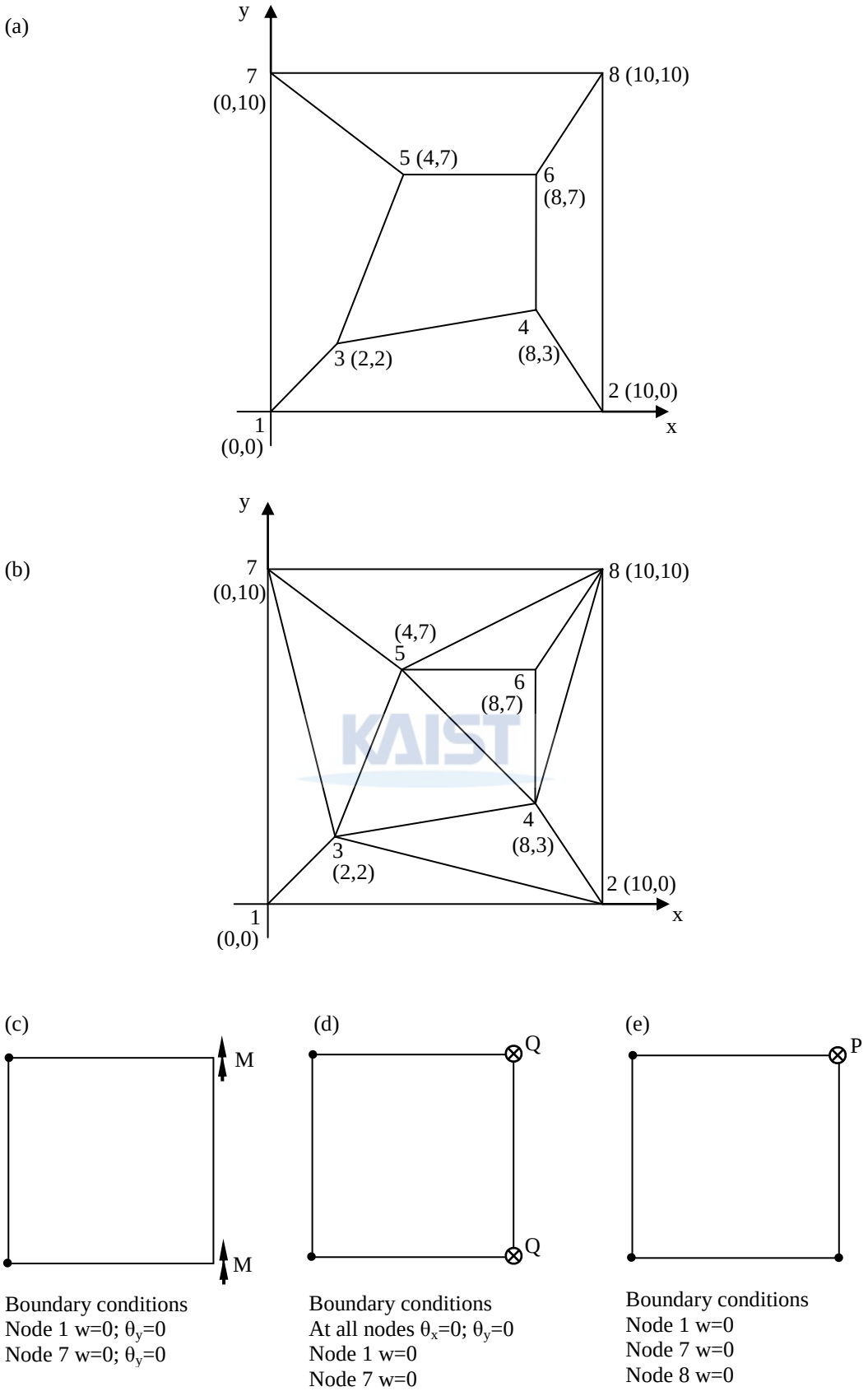

Fig. 3. Patch test. (a) Mesh for quadrilateral element; (b) Mesh for triangular element; (c) Bending case; (d) Shearing case; (e) Twisting case.

• Patch test. The patch test widely used as a test for element convergence, despite its limitations for mixed formulations. We use the test here in numerical form to merely assess the sensitivity of our elements to geometric distortions. The mesh shown in Fig. 3 is for the patch test of 4-node element and 3-node element respectively. This patch of the elements has only constant stress conditions with the minimum displacement boundary conditions and the boundary nodal point forces. If the patch of elements shows the constant stress conditions, the patch test is passed [12-14]. The results of the patch test are presented in Table 5.

• Isotropic element test. The element should be isotropic regardless of the sequence of node numbering. Fig. 4 displays the quadrilateral and triangular element for isotropic test with different nodal numbering. All the input values are the same only except for the connectivity. The results should be exactly the same for all possible tip forces and moments [12]. Table 5 summarizes the results of the isotropic test.

KAIST

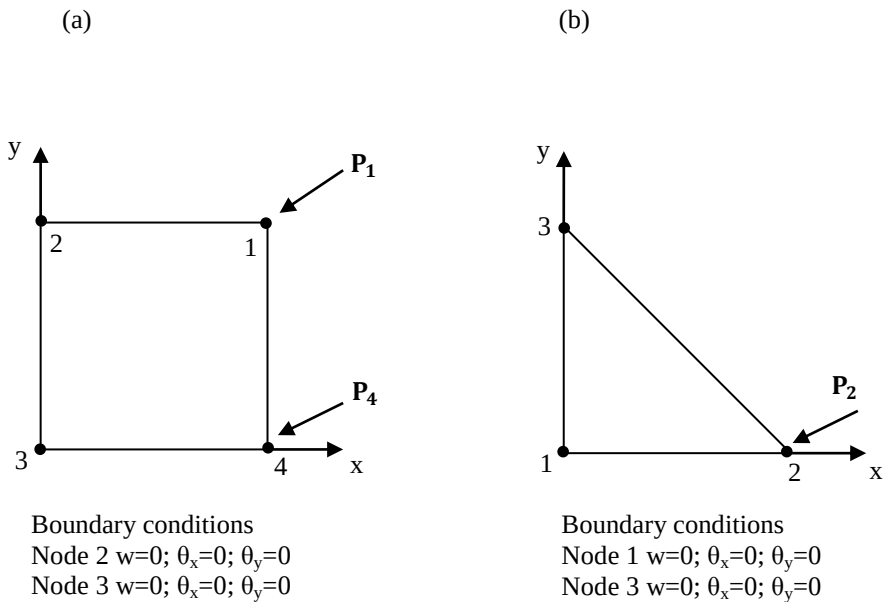

Fig. 4. Isotropic element test. $\mathbf{P_i} = \{f_w, M_x, M_y\}$. (a) 4-node plate element; (b) 3-node plate element.

Table 5. The results of the zero energy mode test, the isotropic element test and the patch test (○:pass).

Test / Plate element	Zero energy mode test	Isotropic Element Test	Patch test		
			Bending Case	Shearing Case	Twisting Case
HR4-CCS	4	○	×	×	×
HR4-LCS	3	○	×	×	○
HR4M-LCS	3	○	○	○	○
HR4M-LCSR45	3	○	○	○	○
HR3-CCS	4	○	×	×	○
HR3-LTCS	3	○	×	×	○
HR3M-LTCS	3	○	○	○	○
HR3M-LTCSR89	3	○	○	○	○

KAIST

3.2. Convergence study

The strain energy is used simply for the convergence study. The reference of the strain energy is obtained by the MITC4 Plate element with a very fine mesh practically

$$\text{relative error} = \frac{E_{ref} - E_h}{E_{ref}} \tag{37}$$

Where E_{ref} is the reference of the strain energy and E_h is the strain energy from the finite element solutions.

3.2.1. Square clamped plate problem

The plate bending problem shown in Fig. 5 considered for the convergence study. The square plate of dimension 2L×2L with the uniform thickness is applied to a uniform pressure normal to the flat surface. All edges are fully clamped. Because the plate is symmetric, we consider only one quarter model(region ABCD shown in Fig. 5) with the following symmetry and boundary conditions imposed [10]

$$\begin{aligned} &\theta_y = 0 \ \text{ along BC,} \\ &\theta_x = 0 \ \text{ along DC, and} \\ &w = \theta_x = \theta_y = 0 \ \text{ along AB and AD.} \end{aligned} \tag{38}$$

Fig. 7-10 display the convergence of the MITC and HR plate elements in the relative error of Eq. (37). The MITC4 plate element with a mesh of 128×128 elements is used for the reference of the strain energy. In the case that the elements have no spurious mode, the convergence curves are drawn. When the meshes are uniform, all the 4-node plate elements are satisfied with the consistency and inf-sup condition in Fig. 7. When the meshes are triangular, the HR3M-LTCSR89 has the better convergence rate than the others in Fig. 8 and 9. As the thickness decreases, the MITC3, HR3M-LTCS and HR3M-LTCSR89 plate elements have shear locking problems even though the elements are contented with the consistency in Fig. 8 and 9. These three triangular elements with cross meshes show the almost optimal convergence in Fig. 10. The HR3-LTCS element is highly locked regardless of the mesh patterns.

3.2.2. Sixty-degree skew plate problem

Fig. 6 shows the sixty-degree skew plate with the uniform thickness subjected to a uniform or variable pressure. All edges simply-supported with w=0 at the edges [10]. Fig. 11-16 show the convergence of the MITC and HR plate elements in the relative error of Eq. (37). The MITC4 plate element with a mesh

of 128×128 elements is used for the reference of the strain energy. The 4-node plate elements are almost satisfied with the consistency and inf-sup condition except for HR4M-LCS in Fig. 11-12. As the meshes are triangular, the HR3M-LTCSR89 has the better convergence rate than the others in Fig. 13-16. When the thickness decreases, the MITC3, HR3M-LTCS and HR3M-LTCSR89 plate elements have shear locking problems even though the elements are satisfied with the consistency. The HR3-LTCS element is highly locked.

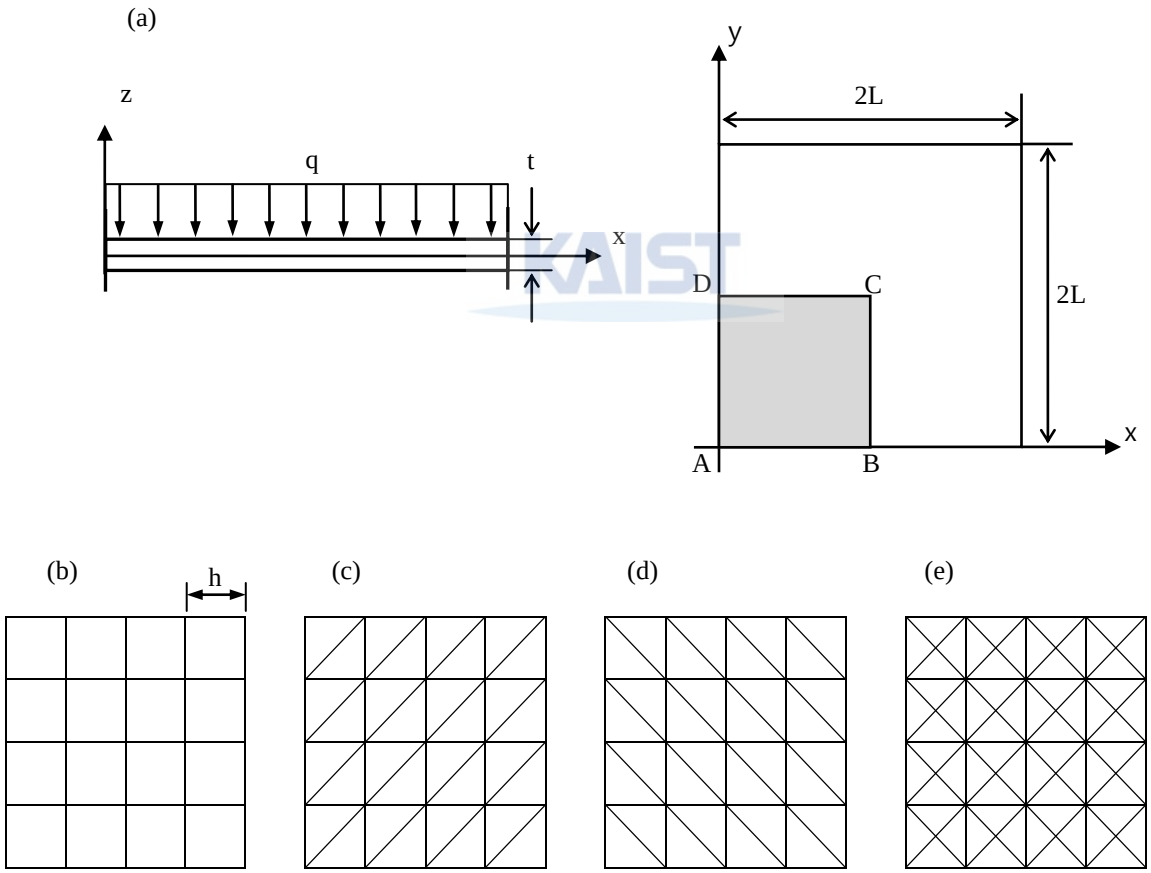

Fig. 5. Square clamped plate problem under the uniform pressure(L=1.0, E=1.7472×10^7, ν=0.3 and q =90). (a) Problem solved; (b) Quadrilateral uniform mesh; (c)Triangular regular mesh-a; (d)Triangular regular mesh-b; (e)Triangular cross mesh.

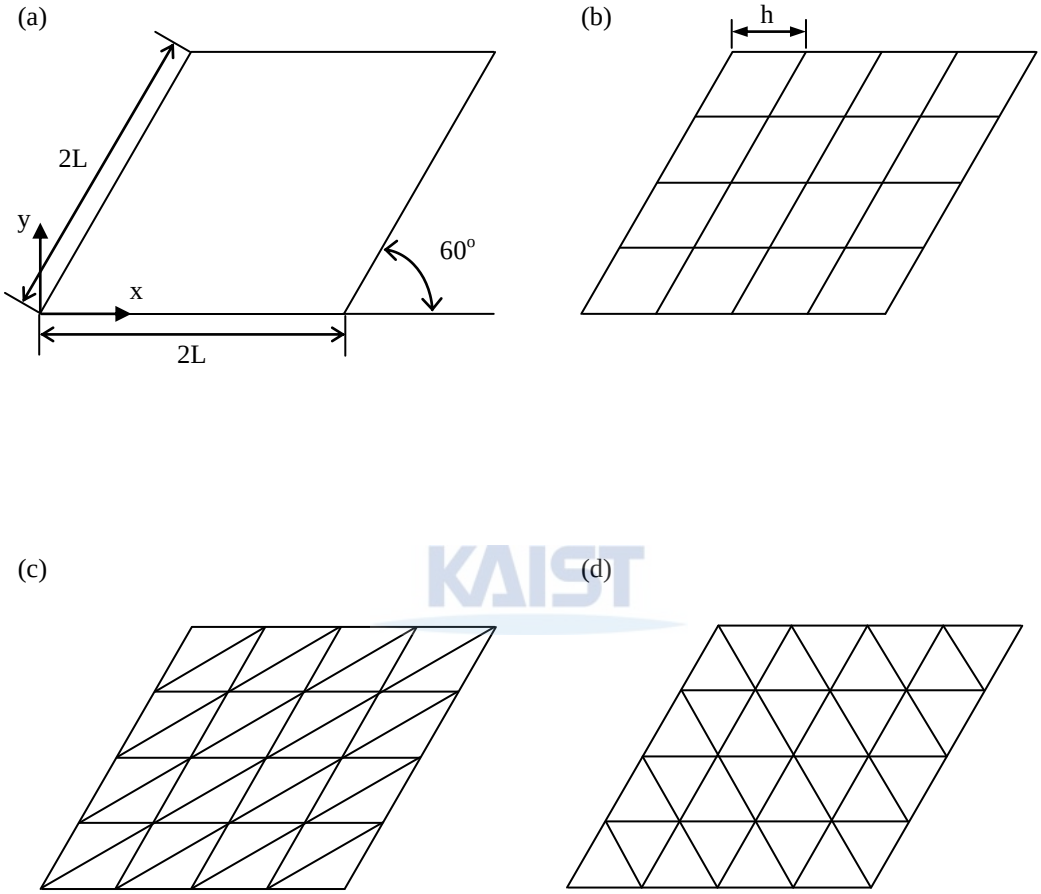

Fig. 6. Sixty-degree skew plate problem(L=1.0, E=1.7472×10^7, ν=0.3 and q = 90, 90xy). (a) Problem solved; (b) Quadrilateral skewed mesh; (c)Triangular skewed regular mesh-a; (d)Triangular skewed regular mesh-b.

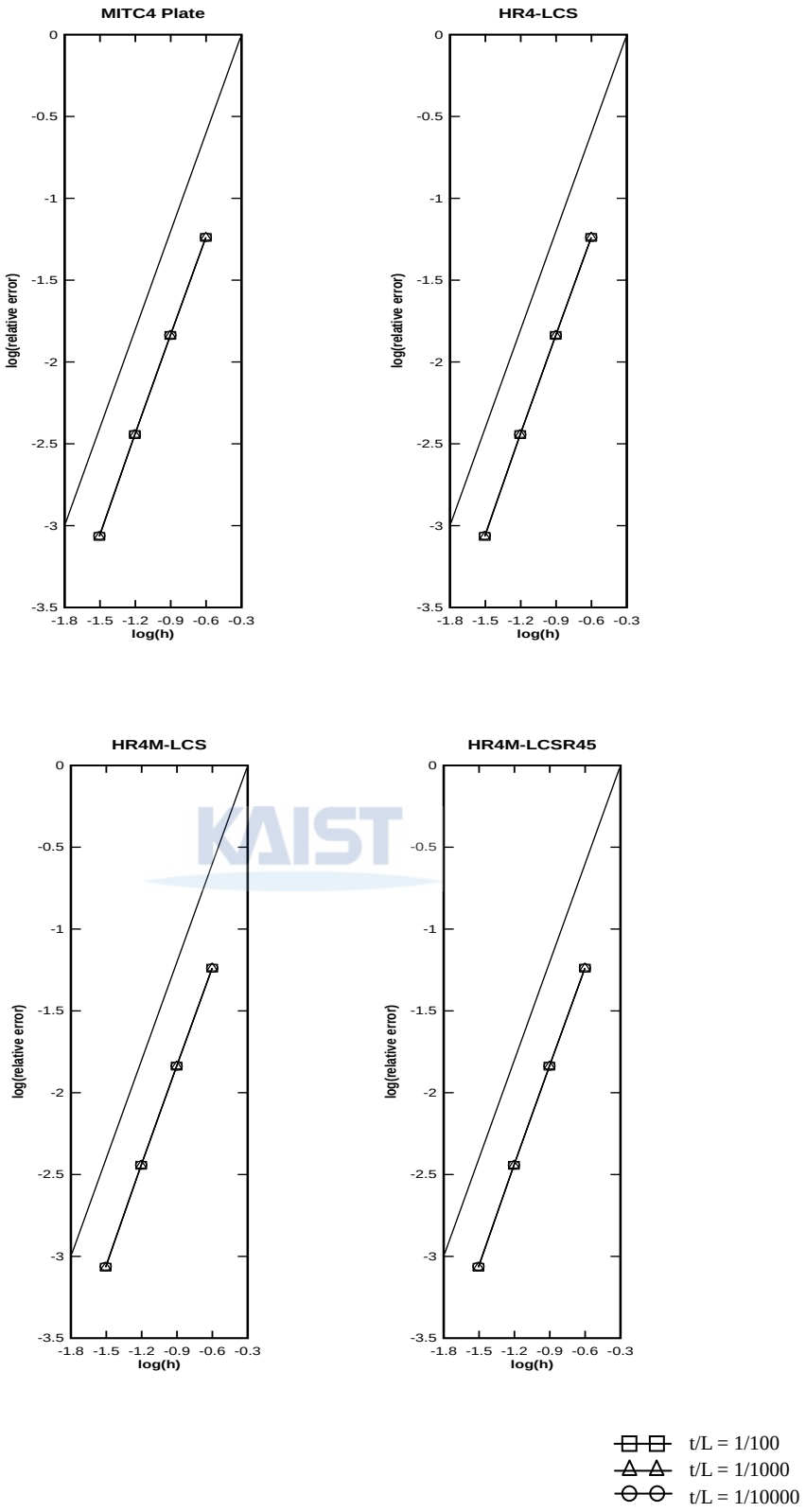

Fig. 7. Convergence curves for the square clamped plate problem. The solid lines show the theoretical convergence rate, which is 2.0. The results come from the quadrilateral uniform mesh in Fig. 5(b).

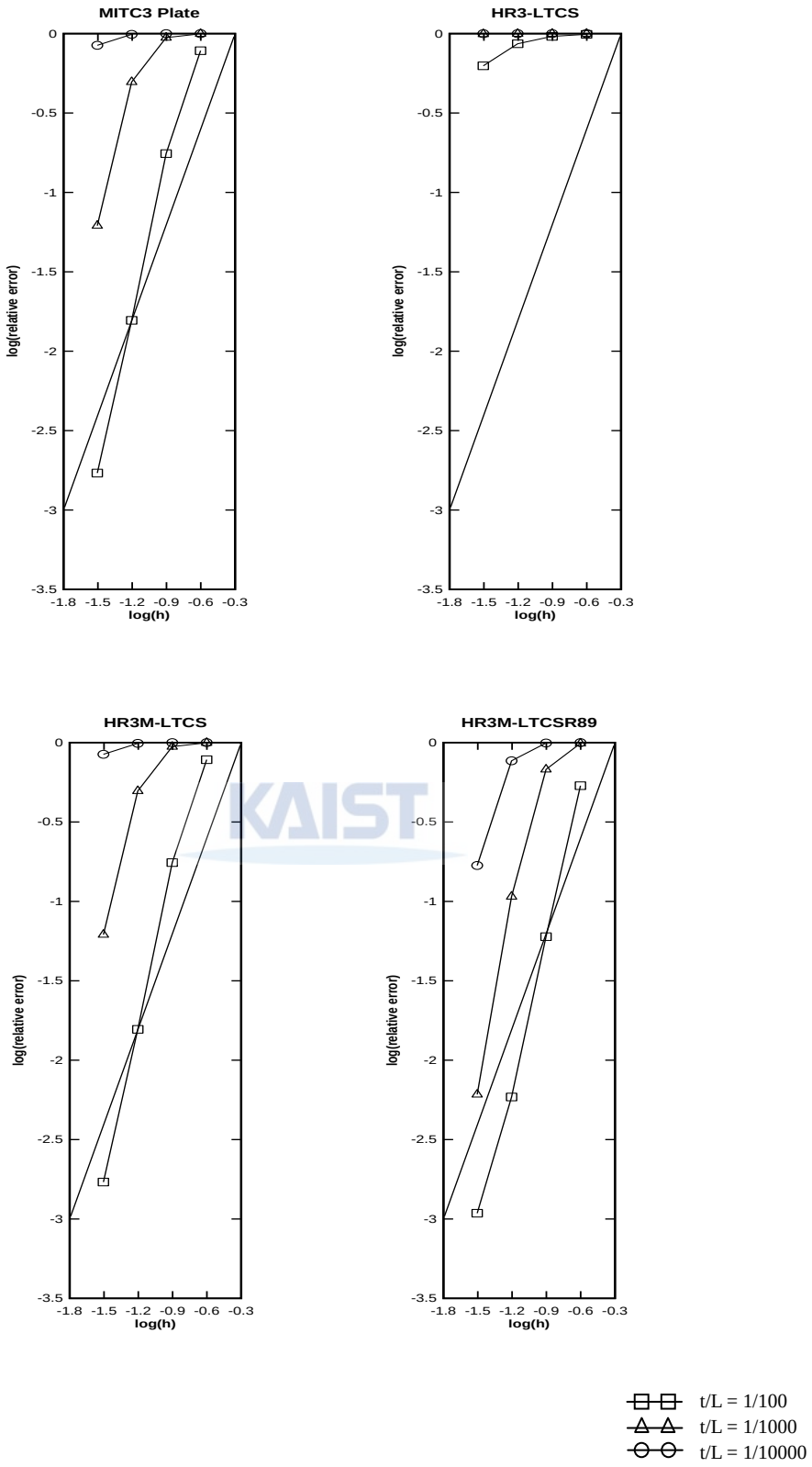

Fig. 8. Convergence curves for the square clamped plate problem. The solid lines show the theoretical convergence rate, which is 2.0. The results come from the triangular regular mesh-a in Fig. 5(c).

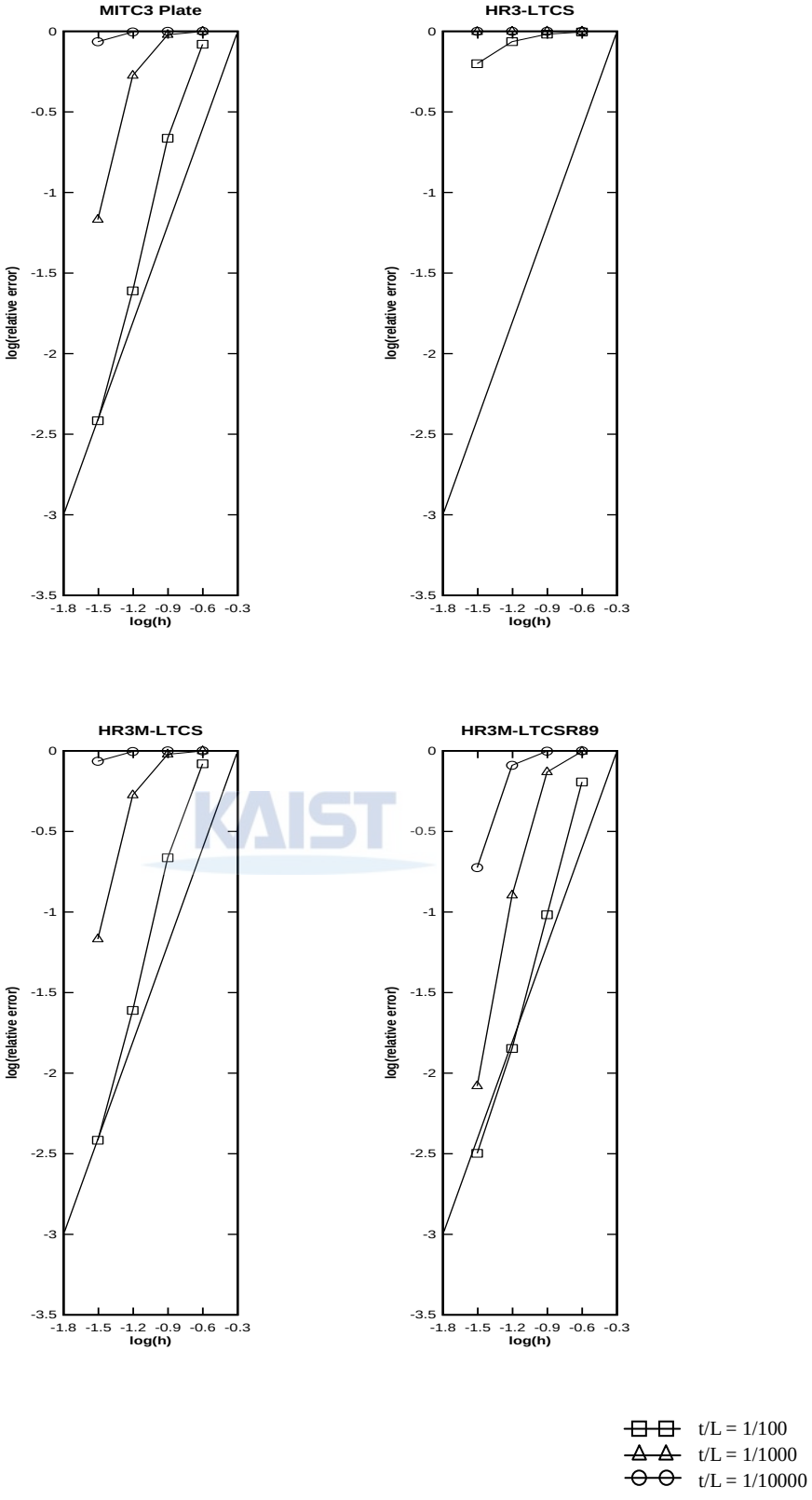

Fig. 9. Convergence curves for the square clamped plate problem. The solid lines show the theoretical convergence rate, which is 2.0. The results come from the triangular regular mesh-b in Fig. 5(d).

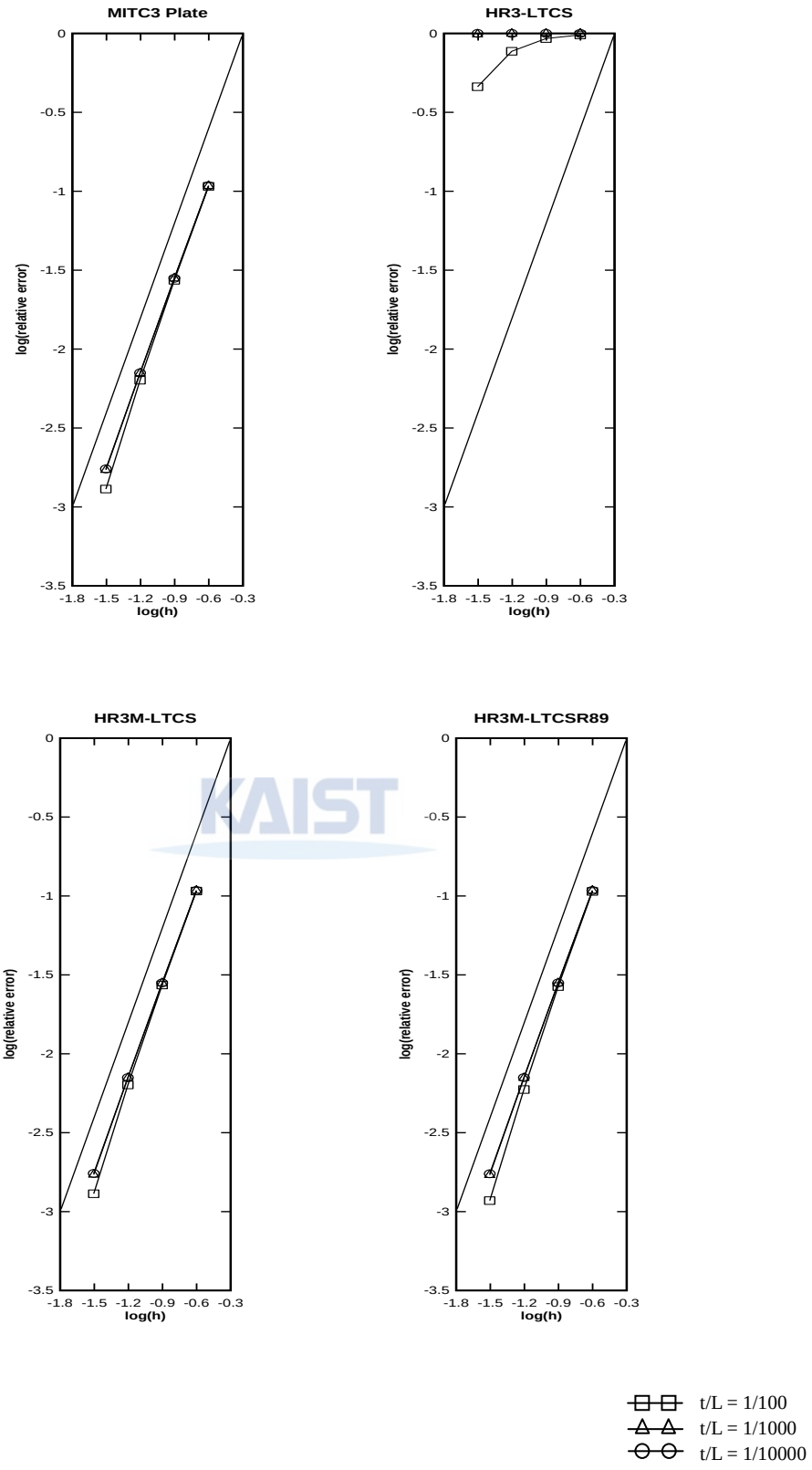

Fig. 10. Convergence curves for the square clamped plate problem. The solid lines show the theoretical convergence rate, which is 2.0. The results come from the triangular cross mesh in Fig. 5(e).

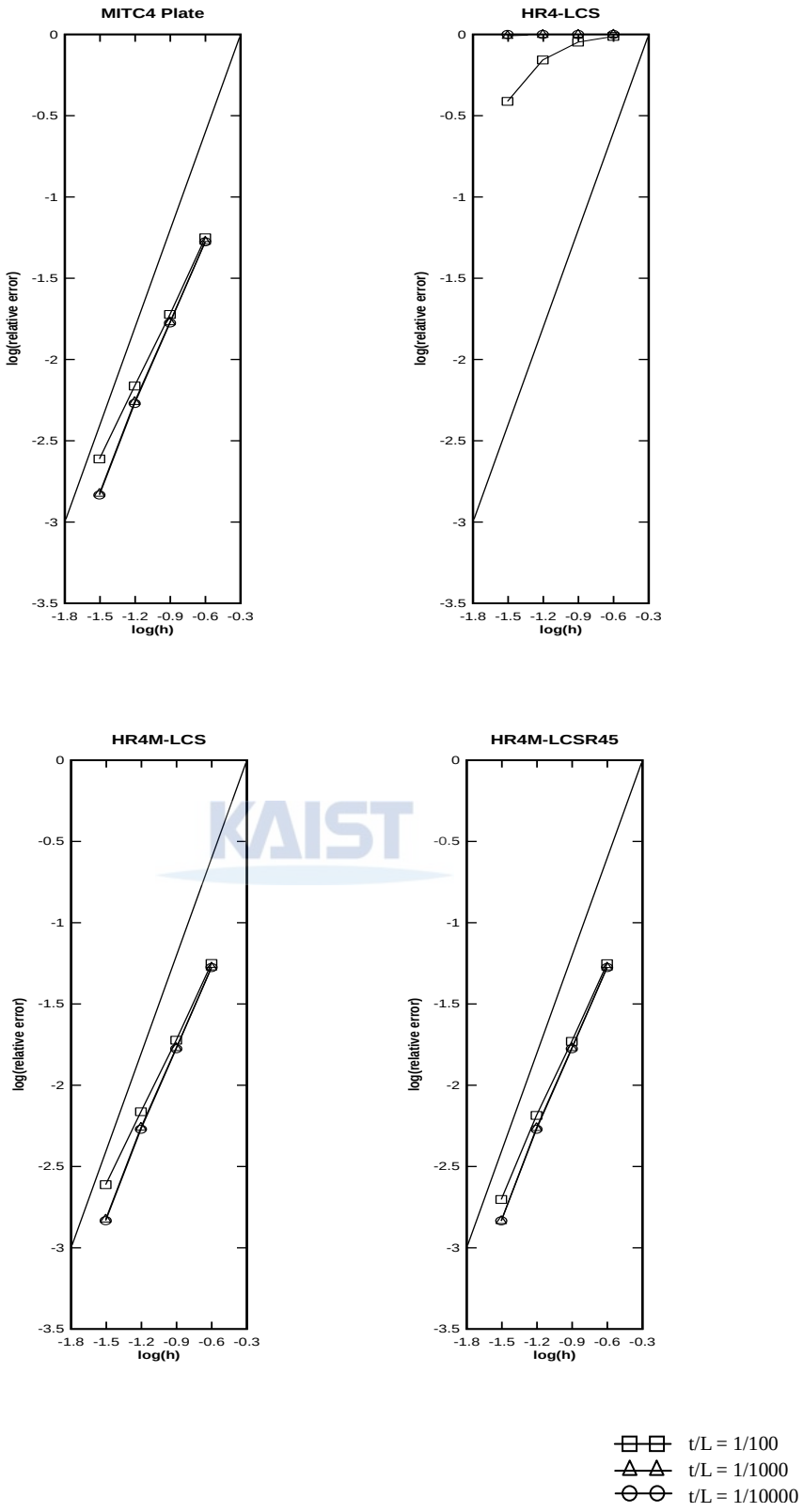

Fig. 11. Convergence curves for the 60^{o} skewed plate problem with the uniform pressure(q=90). The solid lines show the theoretical convergence rate, which is 2.0. The results come from the quadrilateral skewed mesh in Fig. 6(b).

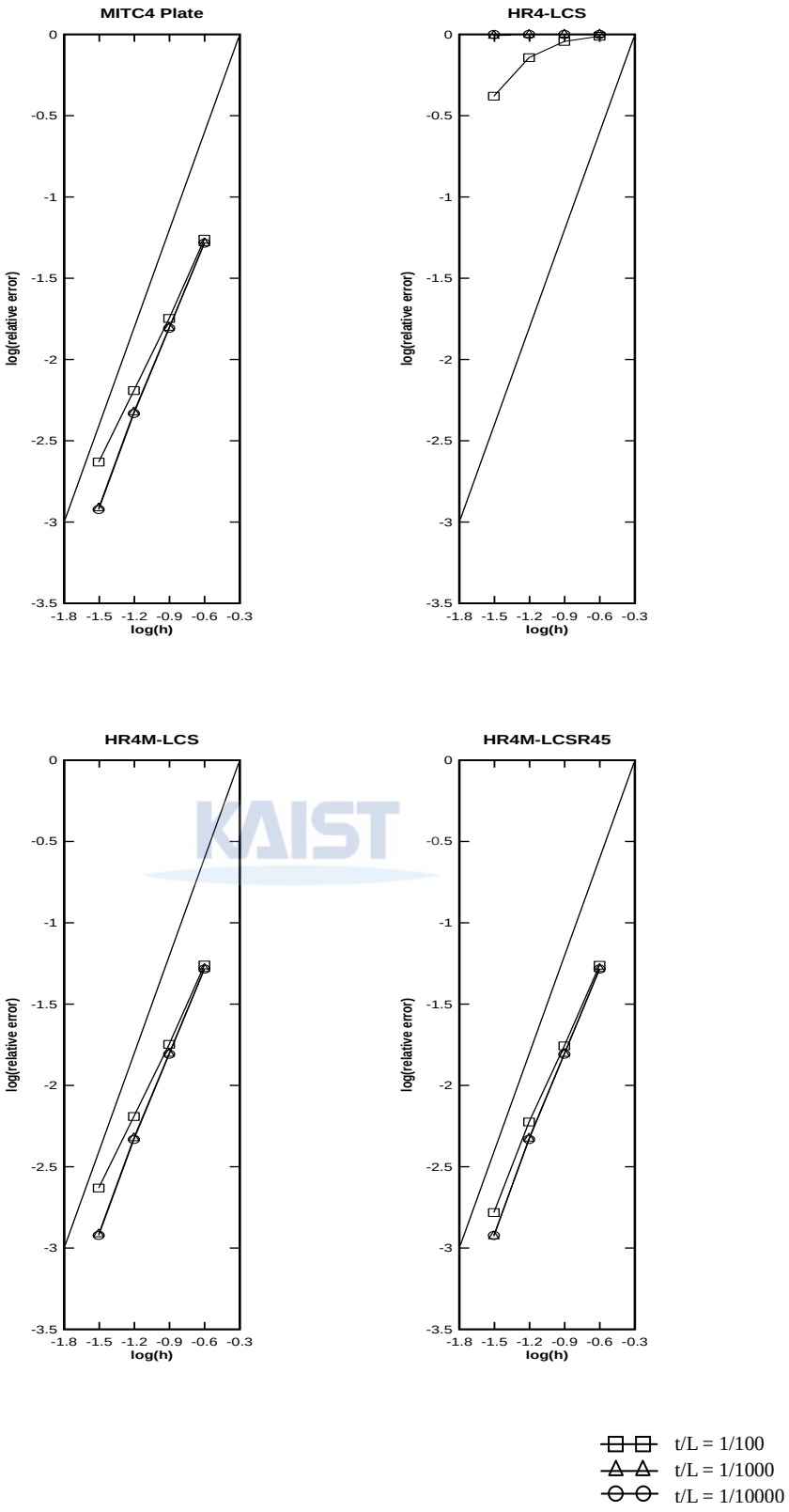

Fig. 12. Convergence curves for the 60^{o} skewed plate problem with the variable pressure(q=90xy). The solid lines show the theoretical convergence rate, which is 2.0. The results come from the quadrilateral skewed mesh in Fig. 6(b).

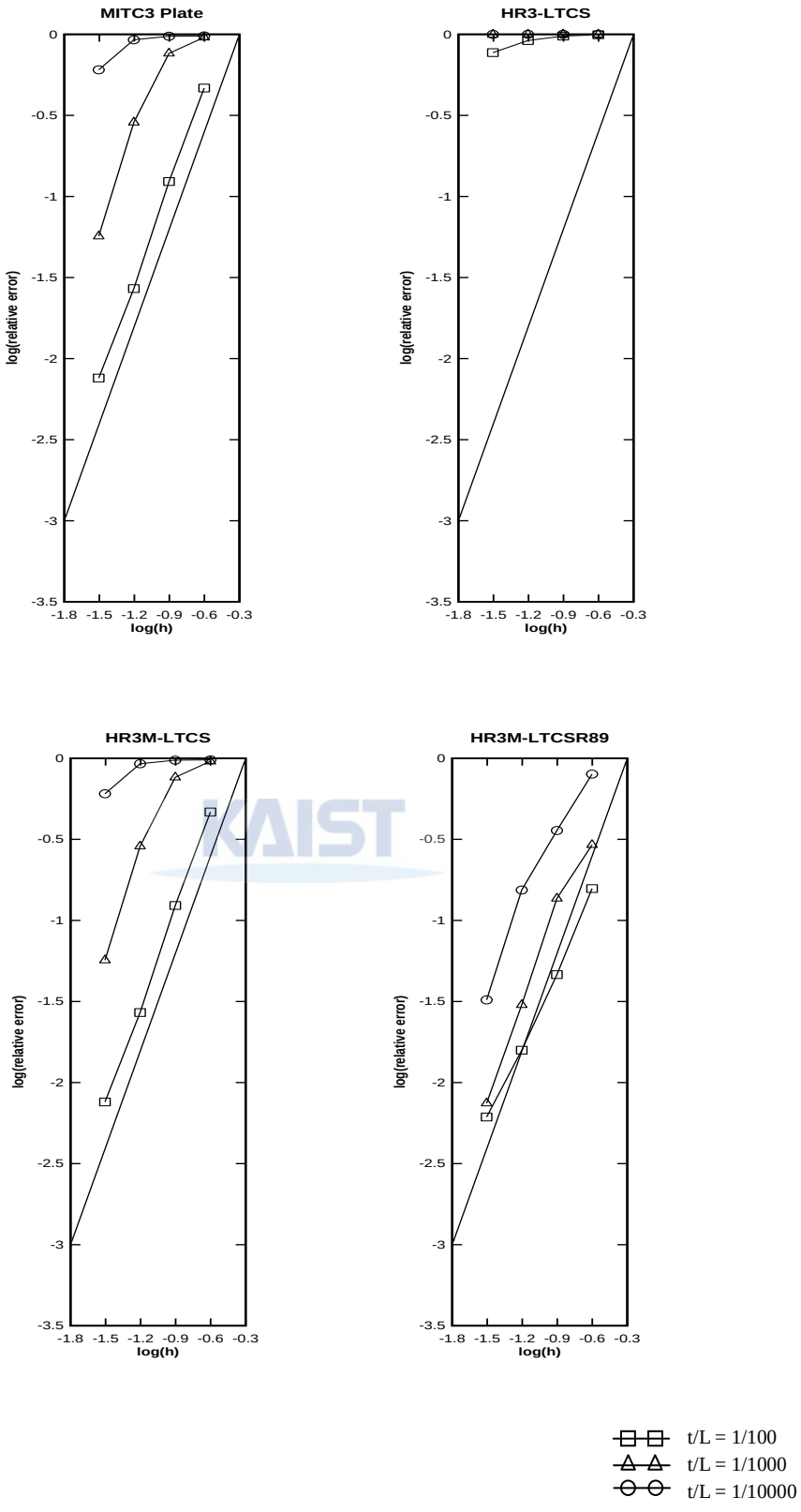

Fig. 13. Convergence curves for the 60^o skewed plate problem with the uniform pressure(q=90). The solid lines show the theoretical convergence rate, which is 2.0. The results come from the triangular skewed mesh-a in Fig. 6(c).

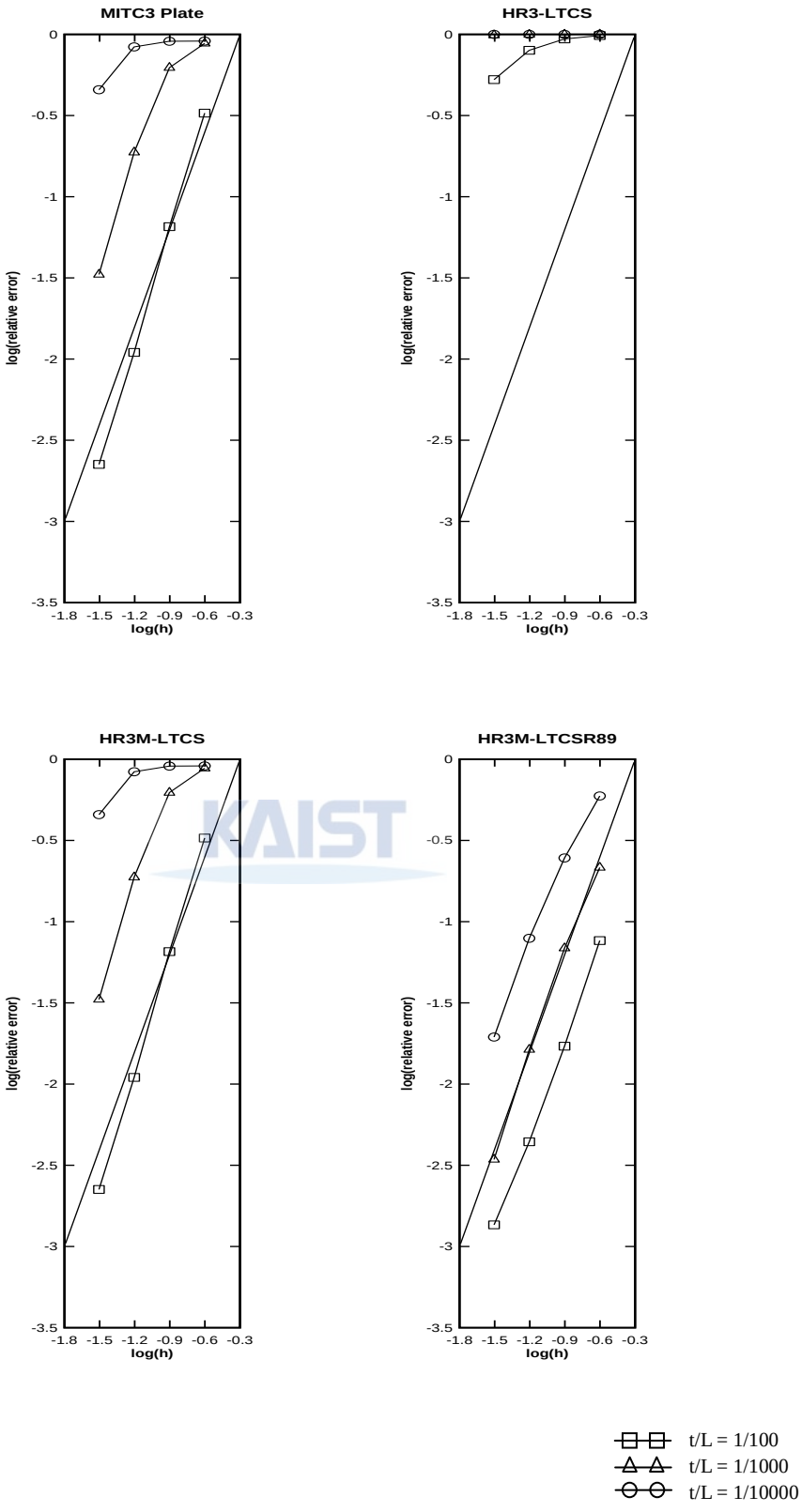

Fig. 14. Convergence curves for the 60^{o} skewed plate problem with the uniform pressure(q=90). The solid lines show the theoretical convergence rate, which is 2.0. The results come from the triangular skewed mesh-b in Fig. 6(d).

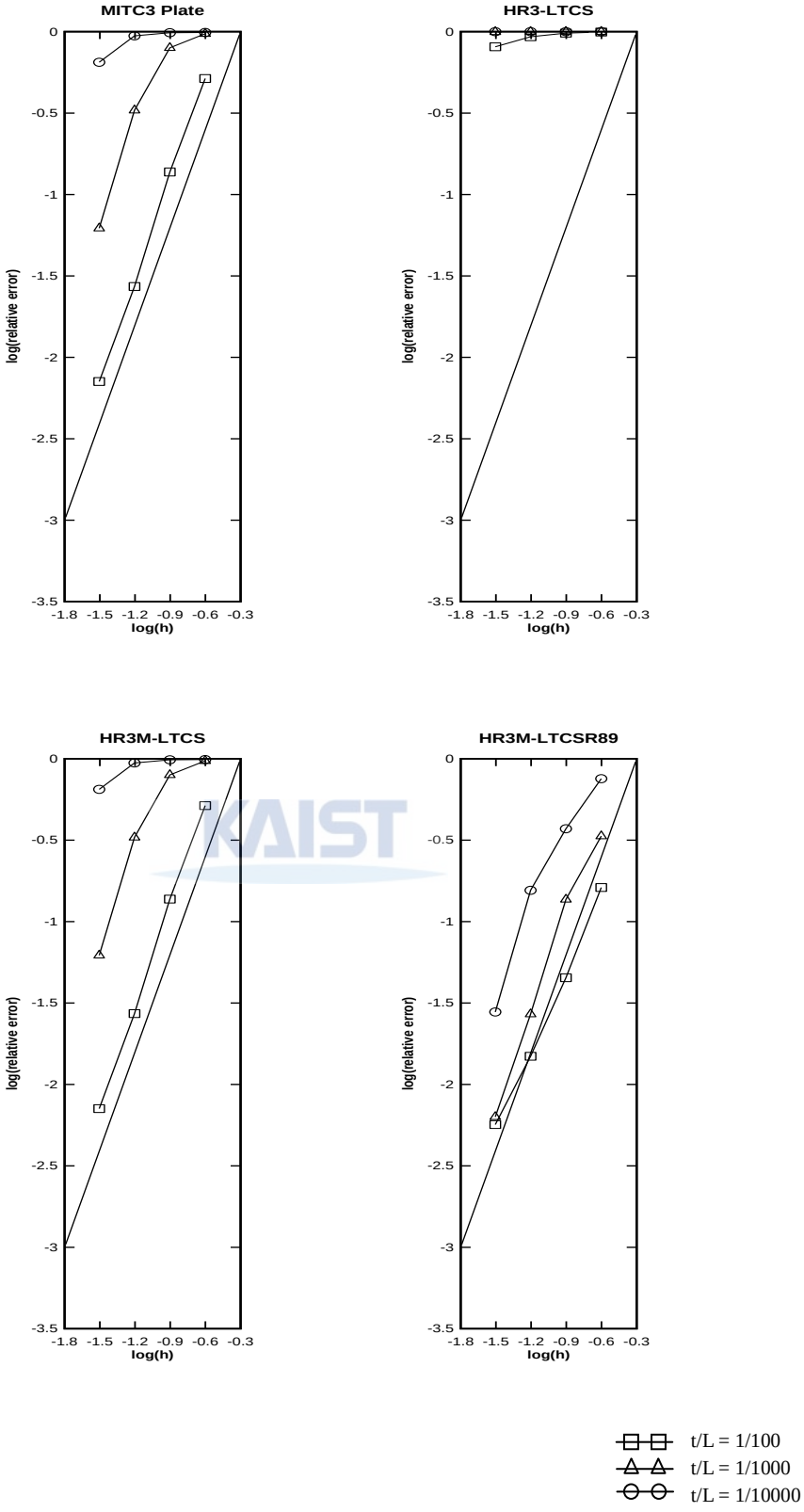

Fig. 15. Convergence curves for the 60^{o} skewed plate problem with the variable pressure(q=90xy). The solid lines show the theoretical convergence rate, which is 2.0. The results come from the triangular skewed mesh-a in Fig. 6(c).

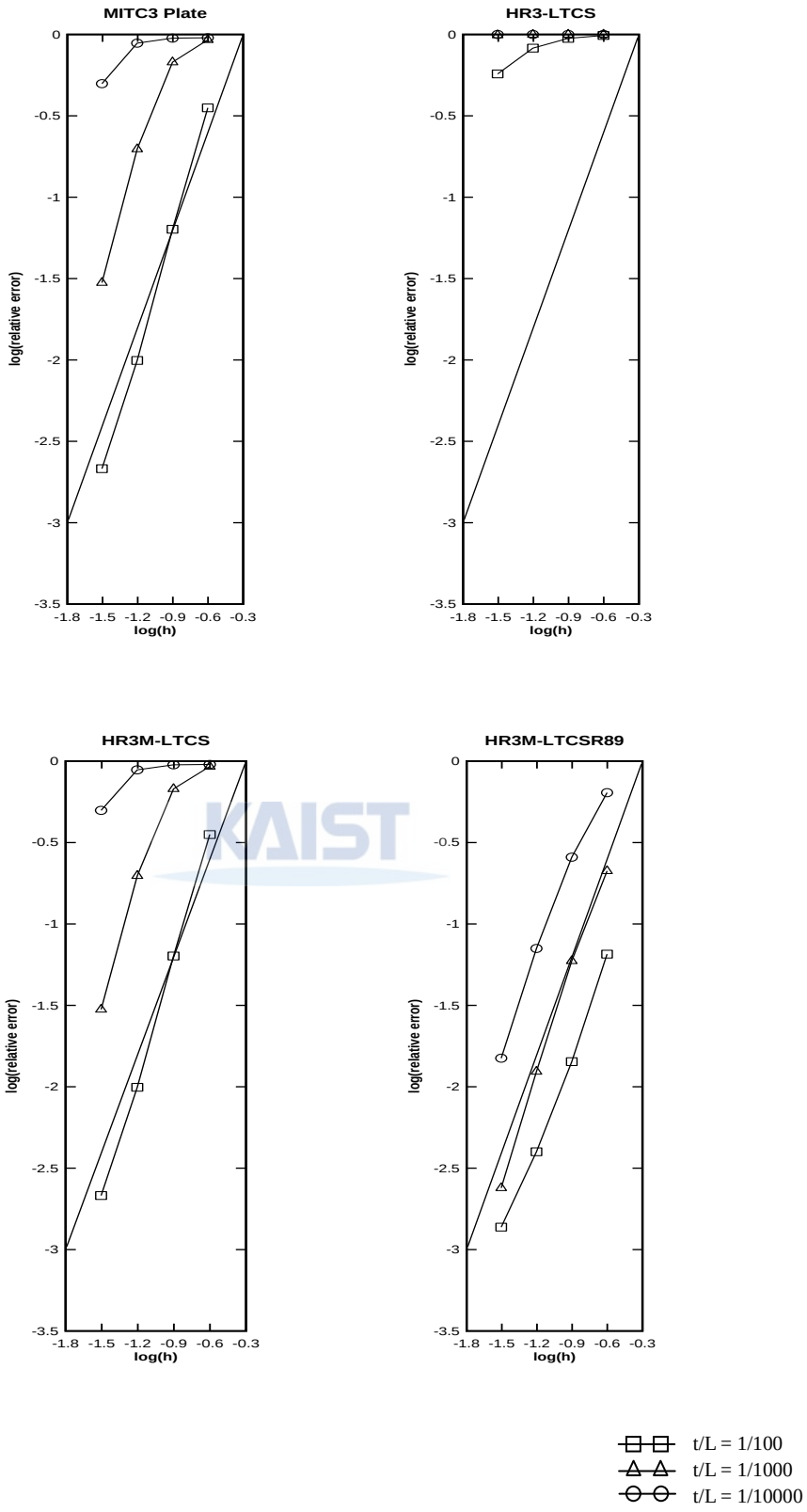

Fig. 16. Convergence curves for the 60^{o} skewed plate problem with the variable pressure(q=90xy). The solid lines show the theoretical convergence rate, which is 2.0. The results come from the triangular skewed mesh-b in Fig. 6(d).

Chapter 4. Conclusions

The objective of this thesis is to develop 4-node and 3-node plate elements based on the Hellinger-Reissner functional to satisfy the practical requirements. The HR4M-LCS and MITC4 plate element, and the HR3M-LTCS and MITC3 plate element are equivalent because the interpolations of the approximated transverse shear strain field that is used to calculate the static condensation for the HR4M-LCS and HR3M-LTCS is the same as the interpolations of the transverse shear strains of the MITC plate elements. The numerical tests show the HR4M-LCSR and HR3M-LTCSR plate elements are more effective than the other plate elements. In particularly, the HR3M-LTCSR89 plate element shows significant improvement for the plate bending problem. This element shows good behavior for the characteristic length(t/L) 1/10 to 1/10000. The HR3M-LTCSR89 plate element can be a reasonable choice to analyze the plate structure in the engineering applications when using triangular meshes. However, it is not uniformly optimal due to the shear locking. So, it is necessary to do more research to develop the ideal 3-node plate element.

KAIST

References

[1] Bathe KJ. Finite element procedures. New York: Prentice Hall; 1996.

[2] Chapelle D, Bathe KJ. The finite element analysis of shells-fundamentals. Berlin: Springer-Verlag; 2003.

[3] Lee PS, Bathe KJ. On the asymptotic behavior of shell structures and the evaluation in finite element solutions. Comput Struct 2002;80:235-55.

[4] Bath KJ, Chapelle D, Lee PS. A shell problem 'highly sensitive' to thickness changes. Int J Numer Methods Eng 2003;57:1039-52.

[5] K. C. Park, G. M. Stanley. A curved C^0 Shell Element Based on Assumed Natural-Coordinate Strains. Journal of applied Mechanics 1986;53:278-90.

[6] Dvorkin EN, Bathe KJ. A continuum mechanics based four-node shell element for general nonlinear analysis. Eng Comput 1984;1:77-88.

[7] Bathe KJ, Dvorkin EN. A formulation of general shell elements - the use of mixed interpolation of tensorial components. Int J Numer Methods Eng 1986;22:697-722.

[8] Bucalem ML, Bathe KJ. Higher-order MITC general shell elements. Int J Numer Methods Eng 1993;36:3729-54.

[9] Bathe KJ, Brezzi F, Cho SW. The MITC7 and MITC9 plate bending elements. Comput Struct 1989;32:797-814.

[10] Lee PS, Bathe KJ. The quadratic MITC plate and MITC shell elements in plate bending. Adv Eng Software 2010;41:712-28.

[11] Batoz JL, Bathe KJ, Ho LW. A study of three-node triangular plate bending elements. Int J Numer Methods Eng 1980;15:1771-1812.

[12] Lee PS, Bathe KJ. Development of MITC isotropic triangular shell finite elements. Comput Struct 2004;82:945-62.

[13] Lee PS, Noh HC, Bath KJ. Insight into 3-node triangular shell finite elements : the effects of element isotropy and mesh patterns. Comput Struct 2007;85:404-18.

[14] Bathe KJ, Dvorkin EN. A four-node plate bending element based on mindlin/reissner plate theory and a mixed integration. Int J Numer Methods Eng 1985;21:367-83.

[15] Hiler JF, Bathe KJ. Measuring convergence of mixed finite element discretizations: an application to shell structures. Comput Struct 2003;81:639-54.

KAIST

Summary

Development of the plate elements based on the Hellinger-Reissner functional

본 논문의 목적은 Hellinger-Reissner 범함수를 이용하여 성능이 향상된 4 노드 와 3 노드 판요소를 개발하는 것이다. Hellinger-Reissner 범함수는 변위와 변형률을 독립적으로 보간 할 수 있게 해준다. 변위법에 의하여 유도된 적절치 못한 변형장을 실제 변형을 반영할 수 있는 변형장으로 대체하고 정적응축을 사용하여 강성행렬을 구하게 된다. 4 노드 판요소인 HR4-CCS, HR4-LCS, HR4M-LCS 그리고 HR4M-LCSR 을 개발하였고, 3 노드 판요소인 HR3-CCS, HR3-LTCS, HR3M-LTCS 그리고 HR3M-LTCSR 을 개발하였다. 이 중에서 HR3M-LTCSR89 판요소는 굽힘상황에서 기존의 3 노드 판요소보다 향상된 성능을 나타내었다.

KAIST